



Intensity Change of NORU (2017) During Binary Tropical Cyclones Interaction

Lu Li¹ · Xuyang Ge¹

Received: 18 September 2019 / Revised: 2 January 2020 / Accepted: 28 January 2020
© Korean Meteorological Society and Springer Nature B.V. 2020

Abstract

In this study, the intensity change of tropical cyclone (TC) Noru (1705) is investigated by using numerical simulations. TC Noru experienced a weakening stage during the binary interaction with TC Kulap (1706). In the presence of Kulap, the model captures well the observed intensity change. On the contrary, once Kulap is removed, it fails to reproduce the weakening stage of Noru. Possible mechanisms are proposed as follows: During the mutual interaction, the competition of moisture supplies will lead to a dry air layer wrapped around Noru. Meanwhile, due to the circulation of nearby Kulap, the vertical shear is relatively larger in the adjacent of Noru. As proposed by previous studies, the negative impacts by dry air layer will be enhanced through two possible pathways. The first is that the dry air directly impacts the TC inner core convection under vertical wind shears. The second is through the downward entropy flux into boundary layer, by which reducing the boundary layer entropy and thus convection. Dynamically, along with the approach of Kulap, it will induce barotropic instability at the outer region, by which greatly enhances the inner-core asymmetry. The asymmetric component will grow at the expense of the mean flow, and thus TC intensity weakens.

Keywords Binary interaction · Tropical cyclone · Intensity change · Barotropic instability

1 Introduction

Under some circumstances, multiple tropical cyclones (MTCs) develop successively over the western North Pacific (WNP). The binary TC interaction was first investigated by Fujiwhara (1921, 1923, 1931). So far, numerous observational (Brand 1970; Carr et al. 1997; Carr and Elsberry 1998; Dong and Neumann 1983; Jang and Chun 2015; Lander and Holland 1993) and numerical studies (Chang 1983; DeMaria and Chan 1984; Holland and Dietachmayer 1993; Prieto et al. 2003; Pokhil et al. 1990; Ritchie and Holland 1993; Schechter 2016; Shin et al. 2006; Wang and Holland 1995) have been conducted in order to understand the so-called Fujiwhara effect. Prieto et al. (2003) identified five types of vortex interactions, including elastic interaction, partial straining out,

complete straining out, partial merger, and complete merger. In practical, the interactions among multiple TCs will lead to a large forecasting track error. As such, most previous studies applied the simple nondivergent barotropic models, and primarily focused on the critical separation distance that determined the mutual attraction or repulsion between two vortices.

Compared with the track changes, the intensity changes during the binary interaction caught less attentions. A few of studies examine the TC intensity changes during the binary TC interaction (Dong and Neumann 1983; Jang and Chun 2015; Wu et al. 2003, 2012; Yang et al. 2008). It is suggested that the merger of binary TCs may cause a dramatic TC intensity change (i.e., rapid intensification). Most previous studies focused on the TC rapid intensification during the mutual interaction. By using numerical simulations, Kuo et al. (2000) found the intensity of TY Zeb (1998) increased after the merging process. However, some cases experienced a weakening process as well. For instance, Ma-on (1106), Wukong (0610) experienced a rapid weakening. On one hand, during the period of binary interaction, the TC likely intensifies rapidly since it absorbs additional vorticity source from the surrounding vortex. On the other hand, the strong outer convection associated with surrounding vortex may prevent the inward transportation of mass and moisture into TC center,

Responsible Editor: Ben Jong-Dao Jou.

✉ Xuyang Ge
xuyang@nuist.edu.cn

¹ Key laboratory of Meteorological Disaster of Ministry of Education, Joint International Research Laboratory of Climate and Environment Change, Collaborative Innovation Center on Forecast and Evaluation of Meteorological Disasters, Nanjing University of Information Science and Technology, Nanjing 210044, China

leading to the collapsing of the inner eyewall. With these regards, the interactions among multiple TCs result in complicated intensity changes, which is a great challenge for the operational forecasting. Hence, the detailed mechanisms need more studies. In this study, the interactions between TC Noru (1705) and Kulap (1706) are selected to reveal the possible underlying mechanisms. Prediction of multiple TCs activity is essential to better prepare for and mitigate TC-induced disasters.

The structure of this paper is organized as follows: Section 2 introduces the observed features of these two TCs. The model configuration and experimental designs are given in section 3. In section 4, the simulated intensity and tracks are compared, and the possible mechanisms accounting for the intensity changes are proposed. Finally, a short summary and discussion is given in the section 5.

2 Observational Analysis

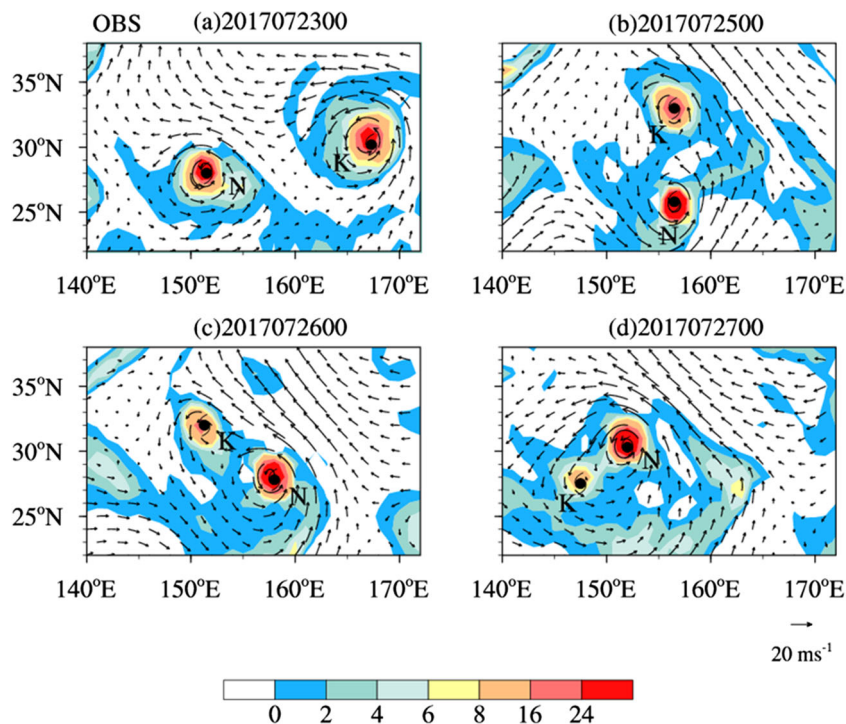
In this study, the binary TC interaction in July 2017 is selected as one example. The observational data is from the best track dataset of Japanese meteorological agency (JMA), which includes 6 hourly TC center location and intensity. During 23–27 July 2017, TC Noru and Kulap existed within the monsoon trough (MT) over the western North Pacific basin (WNP). Figure 1 displays the evolution of 850 hPa circulations of these two storms. In the beginning, TC Kulap is located to the northeast side of the MT, where the easterly flow steers its westward movement. For TC Noru, it is located to the

southern flank of the MT, and moves eastward due to the mean westerly steering flow. With times, these two storms rotated anticlockwise, and gradually approached to each other. Around July 25, Noru shows a sudden northward turning, and then moves westward since July 26 (Fig. 2a).

At 00UTC 25 July, 2017, TC Noru was located to the southwest side of Kulap, with a distance of about 1800 km. This separation distance between two systems is relatively larger than the critical separation distance of Fujiwhara effect suggested by previous studies (Brand 1970; Holland and Dietachmayer 1993; Ritchie and Holland 1993; Shin et al. 2006; Wang and Holland 1995). In those studies, the critical separation distance reflects the distance that two systems start to attract and merge eventually. It is possible that, the critical radius is not only sensitive to the intensity and structure of the systems, but also sensitive to the ambient conditions (i.e., moisture and relative vorticity). Schecter (2016) found that the critical radius is highly sensitive to the ambient relative humidity (RH). In a moister environment, the critical radius tends to become larger. In the current study, these two storms are embedded into the monsoon trough with a higher RH. Hence, the critical radius is likely larger and the partial merger process occurs eventually.

During the period of interest, the intensity of storm Kulap is constantly weaker, with the central minimum sea-level pressure (CMSLP) of 1002 hPa (Fig. 2b). For TC Noru, the intensity increased with CMSLP about 970 hPa at the end of 23 July. Thereafter, it maintained a steady state for about 30 h. Around 06UTC 25 July, as the storm Kulap moved closer to TC Noru, it decayed with a fluctuation of 6 hPa in terms of

Fig. 1 Time evolution of 850 hPa wind (vector; unit: m s^{-1}) and vorticity (shaded; unit: $1 \times 10^{-5} \text{ s}^{-1}$) fields on (a) 23 July, (b) 25 July, (c) 26 July, (d) 27 July, 2017. The letters “N” and “K” indicate NORU and KULAP, respectively



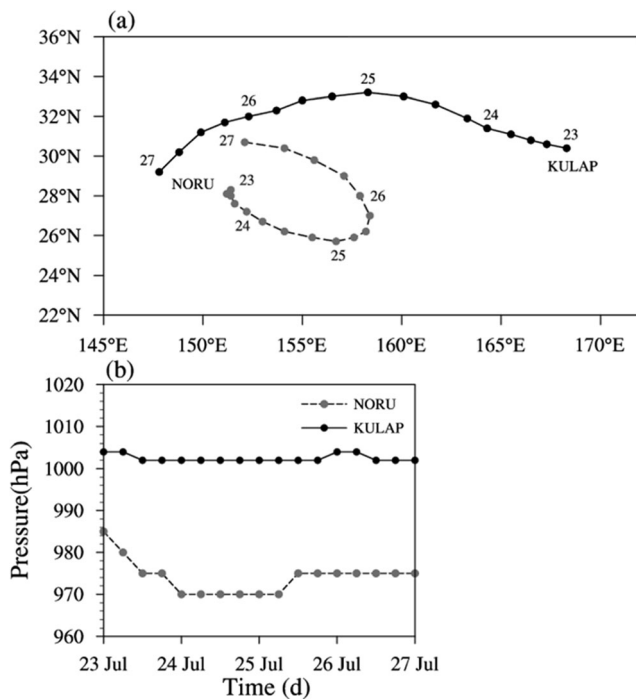


Fig. 2 The JMA (a) best-tracks and (b) minimum centre pressure (CMSLP; hPa) of KULAP (solid line) and NORU (dotted line) from 0000 UTC 23 July to 0000 UTC 27 July

CMSLP. Hence, a question arises here is what responsible for the intensity change of TC Noru? To address this question, a pair of numerical simulations are conducted in the following section.

3 Model and Experimental Designs

In this study, the Advanced Research Weather Research and Forecasting model (ARW-WRF) system version 3.3.1 (Skamarock et al. 2008) is used to conduct numerical simulations. There are 37 levels in the vertical. Three nested domains with the horizontal resolutions of 27, 9, and 3 km are configured. The outermost mesh has grids of 241×181 , the second domain has 271×361 , and the innermost has 241×241 . The model physics includes a microphysics scheme (Ferrier 1994), and Kain–Fritsch convective scheme (Kain 1993). For the radiation process, Dudhia shortwave radiation (Dudhia 1989) and Rapid Radiation Transfer Model (RRTM) longwave radiation parameterization scheme (Mlawer et al. 1997) are used.

The model initial and boundary condition fields are obtained from the 6-hourly $1^\circ \times 1^\circ$ FNL reanalysis data from National Centers for Environmental Prediction (NCEP). The initial time is at 00UTC 23 July, 2017. In the control experiment (CTL), we will attempt to reproduce the track and intensity of the TC Noru (1705). As such, both TC Noru (1705) and Kulap (1706) are kept to include the possible mutual

interactions. In the second experiment (EXP), the weak storm Kulap (1706) is removed by using a spatial filtering technique that is Turkey window method, which is original from the operational COAMPS system of at NRL (Hendricks et al. 2011; Ge et al. 2018). Specifically, the variables with wavelength less than 500 km are firstly extracted, and the components are then removed from the initial fields within a radius of 500 km centered on the minimum sea level pressure (MSLP) of TC Kulap (1706). The comparison likely reflects the potential impacts of a nearby weak storm on the evolution of Noru (1705). The model integrations last for 96 h. More details on the experiment designs are given in Table 1.

4 Simulated Results

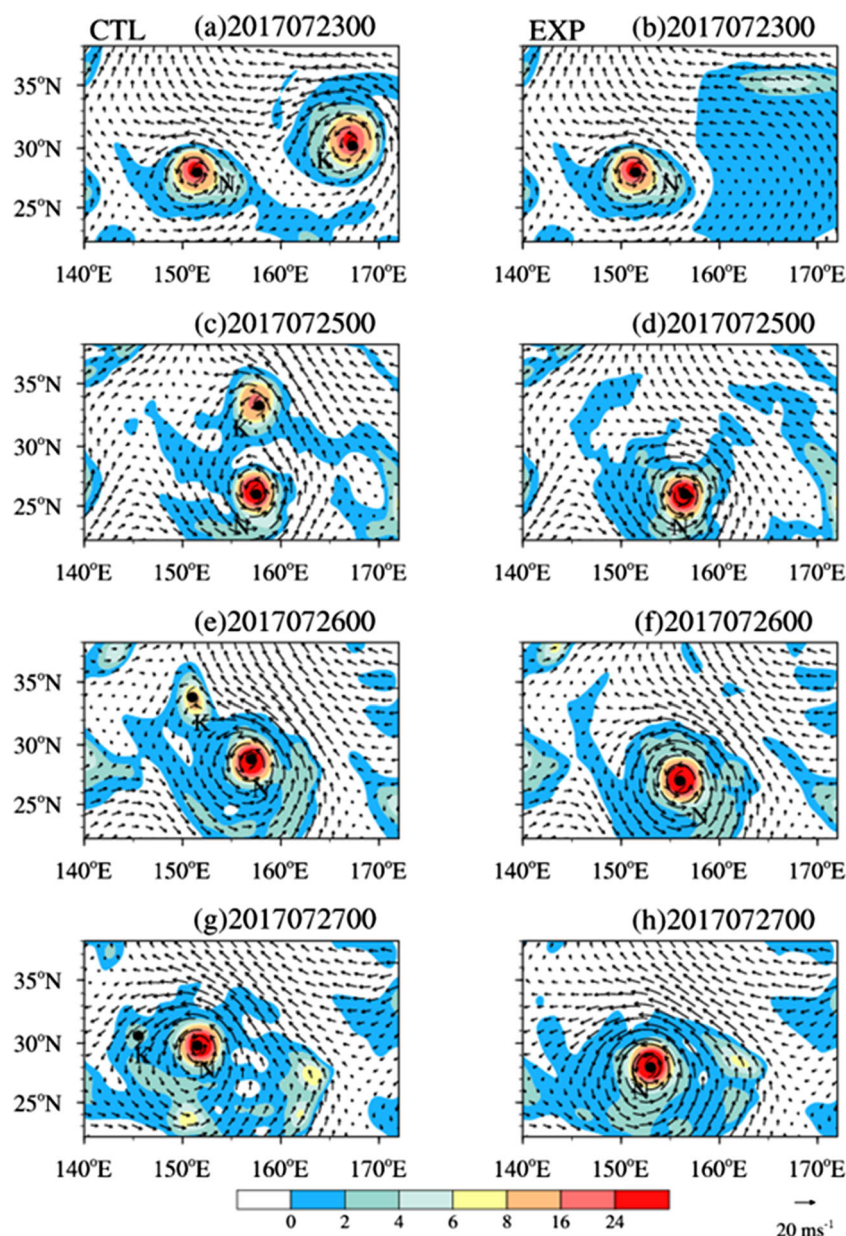
Figure 3 displays the evolution of 850 hPa circulations in CTL and EXP, respectively. In CTL, two storms rotated around each other when they were within about 800 km, and then Noru merged the weaker Kulap eventually. This agrees well with the observation. However, in the absence of the nearby Kulap, the entity experiences a rapid intensification in EXP. Figure 4 compares the simulated track and intensity changes in CTL and EXP, respectively. Basically, the control experiment well simulates the intensity and track changes of TC Noru. That is, the storm initially shows eastward movement, and then experiences a sudden re-curve to be northwestward around 25 July. As such, an arch pattern occurs as observed. In EXP, TC Noru experiences an eastward-northwestward-westward track change as well, except the angle of recurvation is much sharper than that in CTL, indicating a pronounced difference from the observation. Figure 5 displays the evolution of relative positions of two storms centers in CTL. The origin (0, 0) is the middle point between two systems at each time. The result shows a quite symmetrically mutual rotating track, indicating a clear binary interaction.

Nevertheless, there is a marked difference in the simulated intensities of Noru in both experiments. In CTL, the evolution of intensity agrees well with the observation. Specifically, it initially intensifies until at 00UTC 25 July, 2017. Thereafter, it shows a gradually weakening, with a fluctuation of 5 hPa. On the contrary, in the absence of nearby Kulap, TC Noru experiences a rapid intensification. That is, in EXP, it intensifies consistently into a strong TC with the MSLP about 930 hPa at the end of the integration. The sensitivity experiment clearly suggests that the Kulap may suppress the intensification of TC

Table 1 List of experiments

Experiment	Descriptions
CTL	Both NORU and KULAP are kept
EXP	KULAP is removed at the initial time

Fig. 3 Time evolution of 850 hPa wind (vector; unit: m s^{-1}) and vorticity (shaded; unit: $1 \times 10^{-5} \text{ s}^{-1}$) fields on (a) 23 July, (b) 25 July, (c) 26 July, (d) 27 July, 2017, in CTL (left panels) and EXP (right panels), respectively. The letters “N” and “K” indicate NORU and KULAP, respectively



Noru. Hence, we will conduct analyses by using the model output, by which we may gain insights on the underlying processes accounting for the discrepancies.

It has well realized that the ambient moisture is one of the important factors in affecting TC intensity (Gray 1975; Li 2012; McBride and Zehr 1981; Nolan 2007; Tang and Emanuel 2012; Wang 2012). Moreover, previous studies (Kuo et al. 2000; Wu et al. 2012) suggested that the intensity and structure of binary TCs is highly sensitive to the distribution of moisture in between. This motivates us to examine the evolution features of moisture fields in two experiments. Figure 6 compares the time evolution of relative humidity (RH) at height of $z = 4$ km in CTL and EXP, respectively. To have a closer examination on TC Noru, we only focus on the

RH field around this entity. Basically, near-saturated air columns are concentrated around the areas such as inner-core region (i.e., eyewall) and outer spiral rainbands. To the north-west side of the TC, there exists a pronounced dry air rotating cyclonically. With times, the dry air gradually wraps around the TC center, and possibly intrudes into inner core area. This impact of the dry air intrusion is much stronger in CTL, since the band with a smaller RH is much closer to the center.

To further demonstrate the differences, Fig. 7 presents the snapshots of vertical-radius cross sections of RH and equivalent potential temperature (θ_e) at 00UTC 25 July. It is worth to mentioning that these variables are azimuthally averaged. In CTL, there is a clearly relative drier mid-level air layer (i.e., $z = 4\text{--}8$ km) especially beyond the radius of 150 km. This

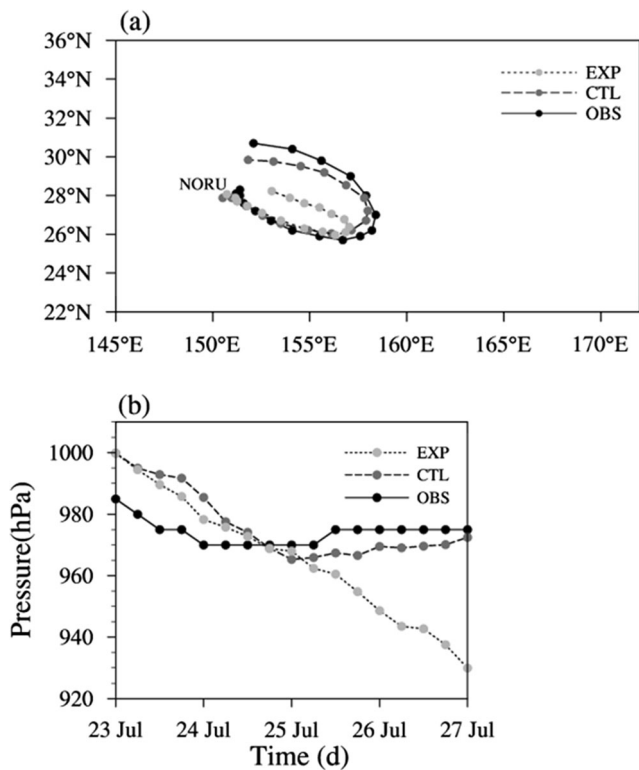


Fig. 4 The JMA and the simulated (a) tracks and (b) minimum center pressure (CMSLP; hPa) of NORU from 0000 UTC 23 July to 0000 UTC 27 July

feature is also identified in the θ_e field. That is, a region with smaller θ_e appears at the mid-level. The region with smaller θ_e is closely associated with the lower RH. The lower mid-level θ_e is considered as one of factors inhibiting TC rapid intensification (Braun 2010; Dunion and Velden 2004; Ge

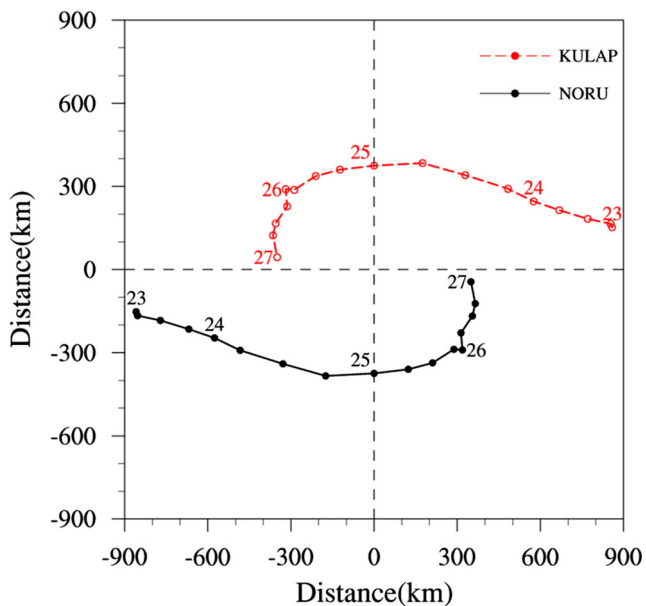


Fig. 5 The evolution of relative positions of the NORU and KULAP centers in CTL during 23 ~ 27 July, 2017. The origin (0, 0) is the middle point between the two Typhoon centers at each time

et al. 2013; Kimball 2006; Wang 2012; Wu et al. 2006; Wu 2007). Physically, dry-air intrusions can have a negative influence on TC intensification as long as the dry air penetrates into inner-core region. This dry air ingestion promotes the formation of cold downdrafts, which transport the air particles with low θ_e into the sub-cloud layer (Emanuel 1989; Tang and Emanuel 2012). Naturally, a question arises here is what causes this dry air intrusion? It is hypothesized that, due to the existence TC Kulap, there is a possible competition on the moisture supply. As a result, the ambient RH around TC Noru is lower in CTL. Of course, the detailed processes resulting in the different ambient RH need more investigations.

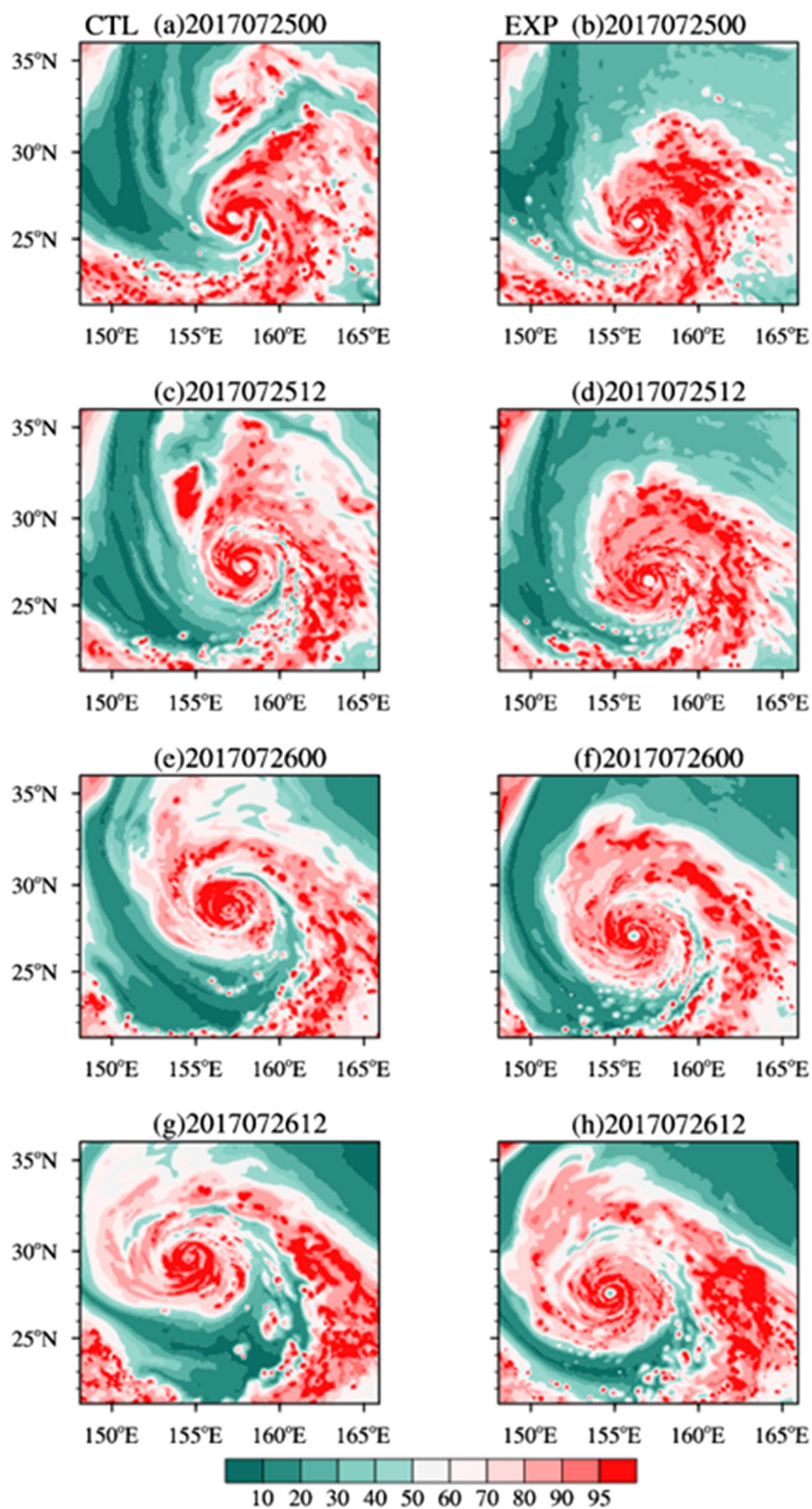
Braun et al. (2012) indicated that the dry air intrusion will lead to prominent asymmetries in convection, and thus inhibits TC intensification. Moreover, it has been recently proposed that a more axisymmetric convective structure is favorable for TC intensification (Miyamoto and Nolan 2018; Miyamoto and Takemi 2013). To this end, the convective axisymmetry (γ) of TC is given as:

$$\gamma(r, z, t) = \frac{\overline{PV}(r, z, t)^2}{\overline{PV}(r, z, t)^2 + \int_0^{2\pi} PV'(r, \lambda, z, t)^2 d\lambda / 2\pi} \quad (1)$$

where γ denotes the potential vorticity axisymmetry index, PV denotes the potential vorticity, r, z, t, λ represent the radius, height, time and azimuth, respectively. The overbar denotes the azimuthal-mean and the prime denotes the deviation from the azimuthal mean. The larger the γ is, the more axisymmetric structure is. Figure 8 compares the time series of γ averaged between $z = 2-8$ km in the vicinity of the eyewall region in both two experiments. γ is averaged over a radial extent of 18 km centered on the TC's RMW at each time snapshot. Broadly, the axisymmetry index increases with time. It is likely that, along with the contraction of RMW, the convection in the TC inner-core region may become more concentrated in a smaller annulus about the TC center. As a result, this contributes to a more symmetric convective structure. In the presence of TC Kulap, the asymmetric structure becomes evident when the dry-air layer is introduced at a smaller distance to the storm center. Namely, the magnitude of γ is much smaller in CTL than that in EXP, which agrees with that the dry air produces marked asymmetries of convection that are unfavorable for a rapid intensification. Overall, TC in EXP has a higher γ than its counterpart during the whole integration period, which agrees well with a rapid intensification rate.

To further illustrate the characteristics of the convection, Fig. 9 gives contoured frequency by altitude diagrams of the vertical velocity (Yuter and Houze 1995), which is obtained within the radius of 180 km centered on the Noru. This method may statistically compare the different behaviors of small-scale convection. Generally, in both experiments, the majority of grid points have small vertical velocities (i.e., $-1 \text{ m s}^{-1} < w$

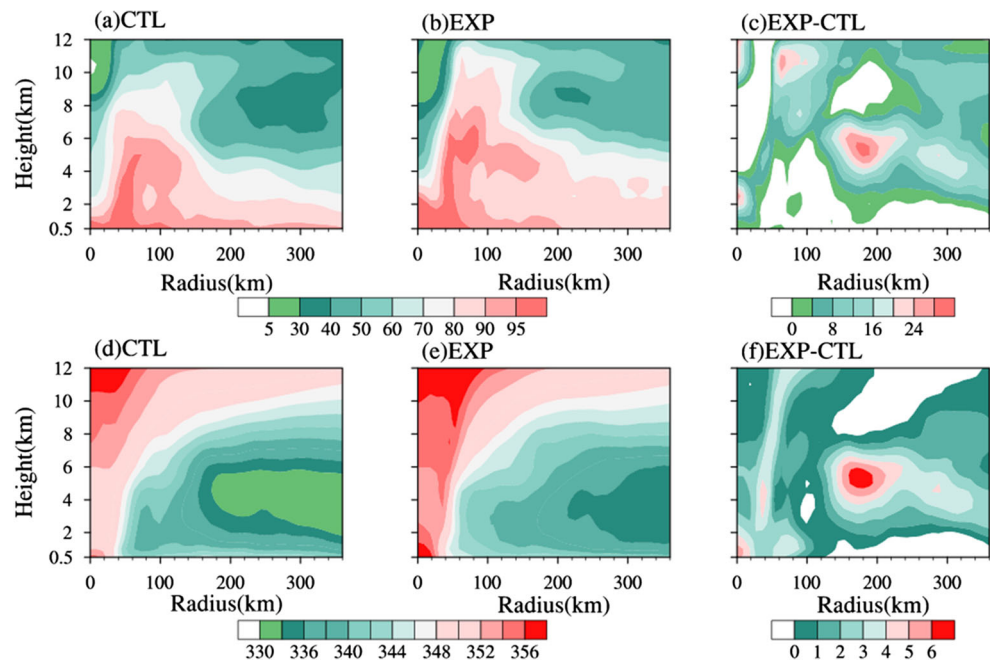
Fig. 6 Evolution of relative humidity RH at the height of $z = 4$ km (shaded; unit: %) fields in CTL (left panels) and EXP (right panels), respectively



$< 1 \text{ m s}^{-1}$). The strong updrafts greater than 2 m s^{-1} only occupy a small region, representing a small portion of vigorous convective bursts. The result is consistent with previous studies (Guimond et al. 2010; Hendricks et al. 2004; Steranka

et al. 1986). At 00UTC 25 July, the portion of strong updrafts are larger in CTL, and decreases with time. This agrees well with the weakening stage of TC Noru during the period of 25–27 July. Nevertheless, the contours with a larger value expand

Fig. 7 Height-radius cross sections of relative humidity RH (upper panels, unit: %) and equivalent potential temperature θ_e (bottom panels, unit: K) fields in CTL (left panels), EXP (middle panels) and difference (right panels) at 0000 UTC 25 July



to right side in EXP, indicating that convective bursts occur more frequently when Kulap is excluded. It is speculated that convective bursts can lead to great latent heat release in the inner-core region where the large inertial stability, by which favors a great conversion ratio of diabatic heating to kinetic energy.

The comparisons demonstrate that a marked difference in the inner-area convective activity. What is the possible mechanism accounting for this discrepancy? Two possible pathways are proposed to explain the low-entropy air penetrates into the eyewall region and then inhibit the TC intensification (Tang and Emanuel 2012). The first pathway is the direct ventilation of low-entropy mid-level air into the eyewall

through turbulent entrainment. For the second low-level pathway, the low-entropy air associated with the convective downdrafts outside the eyewall is advected inwards by the boundary layer radial inflow. Ge et al. (2013) showed that the effect of mid-level dry air intrusion on TC intensification is greatly enhanced in the presence of an environmental VWS. Because of the baroclinic structure, the TC may impose the vertical wind shear (VWS) on its neighboring environment, which is a potential factor in modulating the nearby TC development. This motivates us to examine the VWS in both experiments.

In this study, a spatial filtering technique (Hendricks et al. 2011) is first applied to separate the TC and environmental circulation. The filtering scheme is Turkey window method, which is obtained from the operational system at the Naval Research laboratory. Specifically, the wavelength greater than 500 km is considered as the background flow, and the remaining component (with wavelength shorter than 500 km) represents the TC scale circulation. Thereafter, the mean wind is calculated from 850 to 500 hPa in the vertical, and averaged over a region within a radius of 500 km from the TC center. It should be mentioned that the magnitudes of VWS in both cases are moderate, which are around 5 m s^{-1} (Fig. 10). Nevertheless, the difference of VWS is more significant below 500 hPa. Previous studies (Finocchio et al. 2016; Wang et al. 2015) pointed out that the TC development is probably more sensitive to the lower-level VWS. The flows rotate clockwise with height, indicating a positive helicity that is favorable for TC development (Onderlinde and Nolan 2014; Nolan 2007; Gu et al. 2018). It is suggested that, the height-dependent vortex tilt controls TC structural differences in clockwise (CW) and counterclockwise (CC) hodographs during their

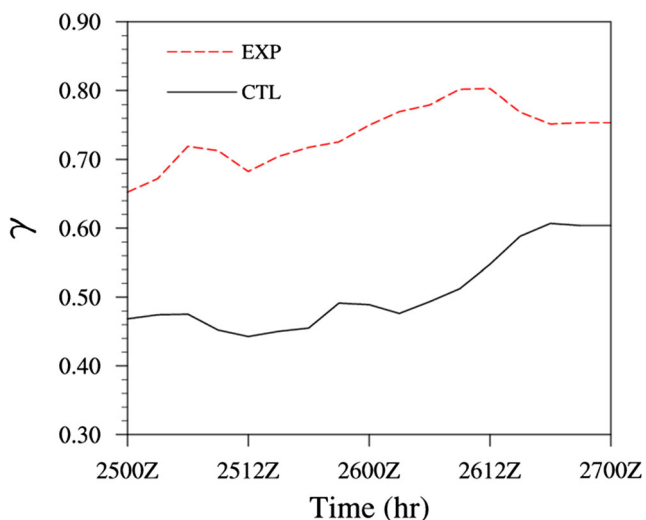
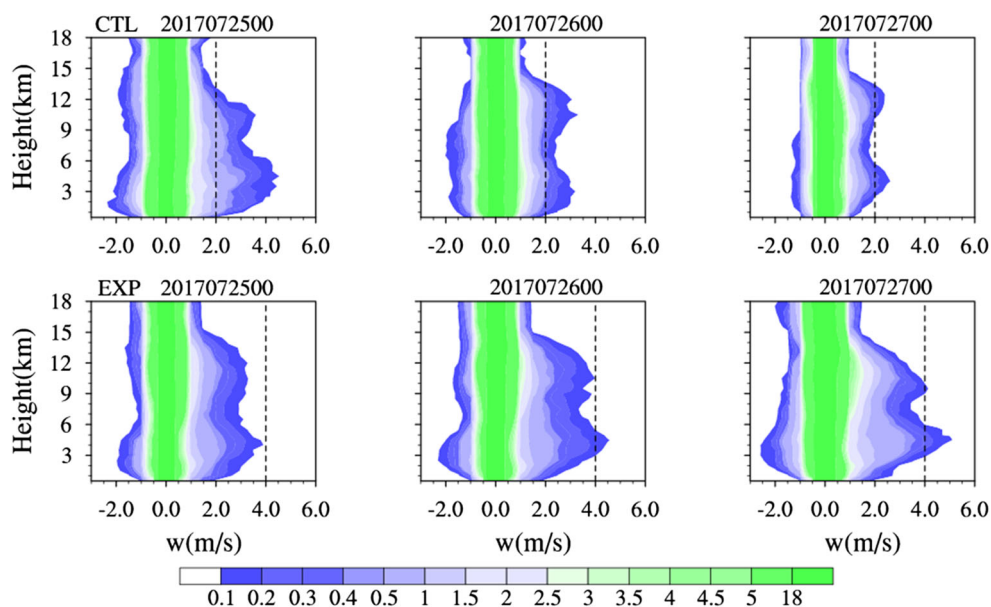


Fig. 8 Time evolution of the axisymmetric PV γ averaged from $z=2$ to 8 km inside the RMW for TC in CTL (black solid), EXP (red dashed)

Fig. 9 Contoured frequency by altitude diagrams of vertical velocity (unit: m s^{-1}) in the innermost 180×180 km domain in CTL (upper panels), EXP (bottom panels) for (left to right) during the period of 25 ~ 27 July. The dotted line is displayed as a reference to highlight the value of 2 m s^{-1} and 4 m s^{-1}



initial stage of development. Moist convection may enhance the coupling between displaced vortices at different levels and thus reduce the vortex tilt amplitude and enhance precession of the overall vortex tilt during the early stage of development. However, differences in the overall vortex tilt between CW and CC hodographs are further amplified by a feedback from convective heating and therefore result in much higher intensification rates for TCs in CW hodographs than those in CC hodographs. The difference of the helicity is small, implying

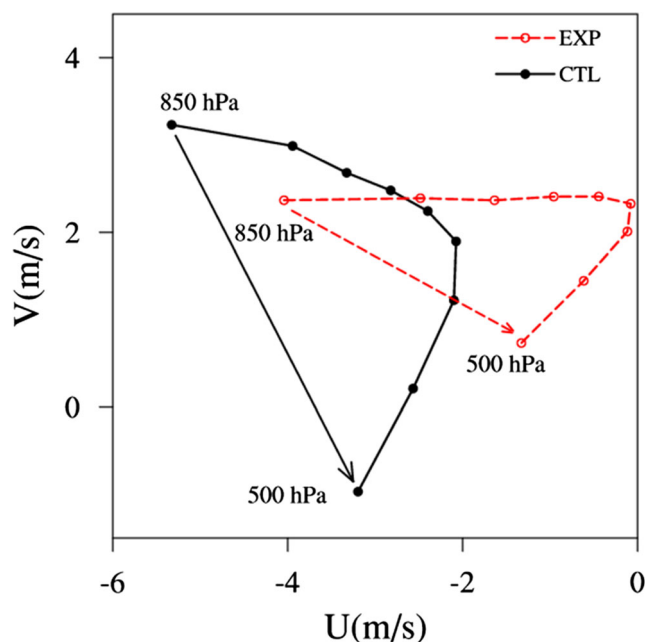


Fig. 10 Simulated hodograph representative of the mean environmental flows in CTL (black solid), EXP (red dashed) during the period of 25 ~ 26 July. The dots represent the wind at each pressure level, and the lines represent the vertical shear between each dot. The arrow represents the vertical wind shear from the bottom (850 hPa) to the top (500 hPa) level

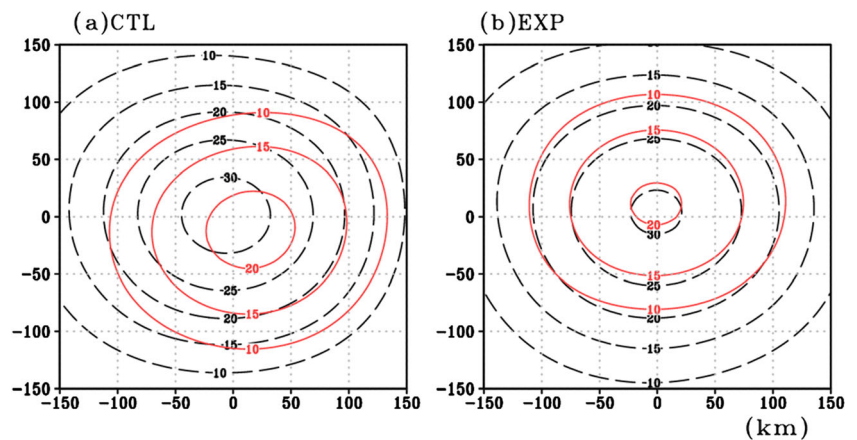
this dynamical impact plays a minor role. Nevertheless, the VWS would result in a vertical tilting. To demonstrate this feature, Fig. 11 compares one snapshot of the vortex centers at the height of $z = 1.5$ km and 7 km in two experiments. In CTL, the mid-level vortex shifts to the downshear side clearly. As such, the horizontal displacement between lower and mid-level vortex is greater than that in EXP, indicating a larger vertical tilting. A vertical alignment favors a greater intensification rate. By this reasoning, this partially accounts for the difference in the intensity change.

Riemer et al. (2013) suggested that the low-entropy air brought into the boundary layer from above by shear-induced downdrafts may significantly reduce the equivalent potential temperature in boundary layer, and subsequently constrain the storm intensity when the lower-entropy air enters the eyewall updrafts. This effect is quantitatively measured by using the downward entropy flux (DFX), which is defined as

$$DFX = w_- \cdot \theta'_e$$

where w_- is the downward motion, θ'_e is the perturbation that is deviated from the azimuthal mean. Hence, the positive DFX reflects downward flux leading to a reduction of entropy in the boundary layer. The low θ_e implies a weaker thermal efficiency of Carnot heat engine. To this end, Fig. 12 presents the snapshot of horizontal distribution of DFX during 24 ~ 26 July. In CTL, the anomaly positive DFX initially occurs at the northwest quadrant, and moves cyclonically to southeast side at 12UTC 26 July. In CTL, the positive value dominates in the downshear-left quadrant, and the general distribution of DFX is consistent with Riemer et al. (2013). During this period, this positive DFX is organized into a clear band-like structure. As such, a clear wavenumber 1 asymmetry is evident. The enhanced DFX is largely collocated with the dry

Fig. 11 The simulated upper- (7 km; red contour) and lower- (1.5 km; black contour) level vorticity fields (unit: $1 \times 10^{-5} \text{ s}^{-1}$) at 0000 UTC 26 July in (a) CTL and (b) EXP. Only vorticity fields associated with wavelengths $>200 \text{ km}$ are shown

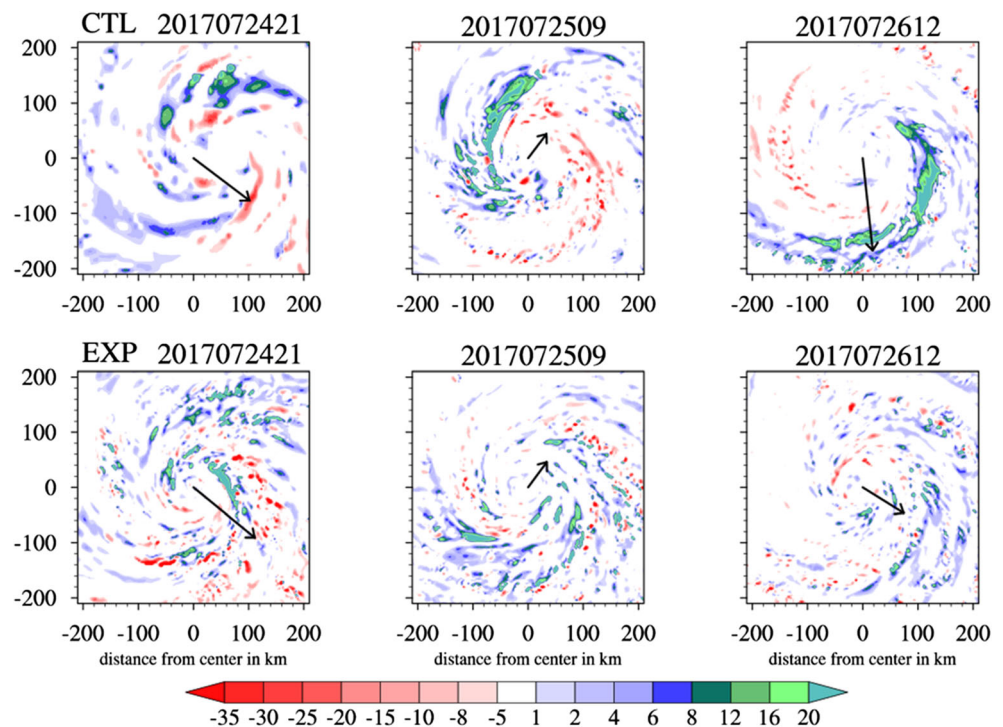


intrusion, implying a potential impact of mid-level dry air on the thermodynamical conditions in the boundary layer. It is likely that, in the presence of mid-level dry air, it will enhance the evaporative cooling and thus the downdrafts (Dunion and Velden 2004). Accordingly, it leads to a lower θ_e therein. In turn, the enhanced evaporative cooling will induce greater downdraft as well. In contrast, in EXP, the spatial pattern of positive DFX is much weaker or less organized. The result is also consistent with the a larger axisymmetry index in EXP. In short, the stronger positive DFX, the greater reduction of entropy in the boundary layer. As a consequence, the TC intensification will be greatly suppressed in CTL.

In CTL, TC Kulap approaches gradually and then actually merges with TC Noru. During the approach period, it is greatly deformed. Within the axisymmetric dynamical framework,

the relative vorticity associated with Kulap circulation may induce a local vorticity maximum at a certain radius. As such, the signs of the radial gradient of vorticity change in the adjacent of this local maximum, which satisfies the necessary condition of barotropic instability. Recent literatures (Peng and Reynolds 2006; Peng et al. 2009; Yan et al. 2019) examined the impacts of barotropic instability at outer region on the TC intensification. It has been proposed that, the emergence of barotropic instability at the outer region could increase the asymmetry in the inner area, which is ascribable to the interaction between the perturbations at inner and outer regions. As a consequence, the enhancement of inner-core asymmetric component will affect the TC intensification. To this end, we examine the time evolution of the radial profile of relative vorticity in two experiments (Fig. 13). Apparently, there exists

Fig. 12 Time evolution of DFX (unit: 0.1 K m s^{-1}) at the top of the inflow layer in CTL (upper panels), EXP (bottom panels) for (left to right) at 2100 UTC 24 July, 0900 UTC 25 July and 1200 UTC 26 July. The arrow represents the vertical wind shear from the bottom (850 hPa) to the top (200 hPa) level



a local vorticity maximum in CTL, although the magnitude is quite smaller compared to that in the inner core region (i.e., eyewall area). More specifically, in CTL, the local vorticity maximum is located at the radius of 900 km at 00UTC 25 July, and then moves into the radius of 700 km away from the Noru center at 12UTC 26 July. In contrast, the vorticity decreases gradually with the radius, and thus there is barotropic stable in EXP. The comparison indicates that this outer barotropic instability is ascribed to TC Kulap.

Following Yan et al. (2019), the wave-number two component of relative vorticity field is extracted (Fig. 14). Notice that the wavenumber-2 asymmetric components exist in the inner area in both experiments. During the period of interest, the asymmetric perturbations in CTL are much pronounced compared with those in EXP. Moreover, the magnitude increases significantly with times. It is speculated that, the enhancement of asymmetric eddies grows at the expense of the mean flow, and thus the TC intensity weakens. The greater asymmetric components likely account for the lower axisymmetry index (γ) as shown in Fig. 8.

To further examine the evolution of asymmetric components, the amplitudes of wavenumber (WN#) 1 and 2 in the two experiments are examined in Fig. 15. The asymmetry is likely attributed to the VWS (i.e., WN#1) and barotropic instability (i.e., WN#2). During the period of interest (i.e., 1200 UTC 24 July – 1200 UTC 25 July), the amplitude of WN#1 is relative larger compared with that of WN#2, indicating that the importance of the VWS effect at the early stage.

Nevertheless, the amplitude of asymmetric perturbations increases significantly with times and attains peak at 0000 UTC 25 July in CTL, whereas the peaks appear at 0600 UTC 24 July in EXP. For the WN#2 component, its peak appears around 0000 25 July as well, and is more pronounced in CTL, suggesting that the impacts of the outer barotropic instability. Thereafter, the amplitudes of both WN#1 and WN#2 are relatively larger in CTL than that in EXP. With this regard, both processes should work together in leading to a slow intensification rate. In this study, we cannot tell the relative contribution of these asymmetries, since the complicated non-linear interactions exist therein. This tropic awaits further studies.

5 Summary and Discussion

In this study, the intensity change of TC Noru (1705) is simulated to understand the possible processes related to the binary TC interaction. A pair of numerical simulations are conducted. In the presence of TC Kulap, the simulation captures well with the observation. Namely, TC Noru initially develops rapidly, and then weakens during the latter stage. In contrast, in the absence of Kulap, TC Noru experiences a consistently rapid intensification process. The possible mechanisms accounting for the intensity change are summarized as the follows:

Fig. 13 Evolution of radial profiles of azimuthal mean relative vorticity fields (unit: $1 \times 10^{-5} \text{ s}^{-1}$) in CTL (black solid), EXP (red dashed) for (left to right) at (a) 0000 UTC 25 July, (b) 1200 UTC 25 July, (c) 0000 UTC 26 July and 1200 UTC 26 July at the height of $z = 1.5$ km. And the small pictures represent the blue box area within the radius from 300 to 1000 km

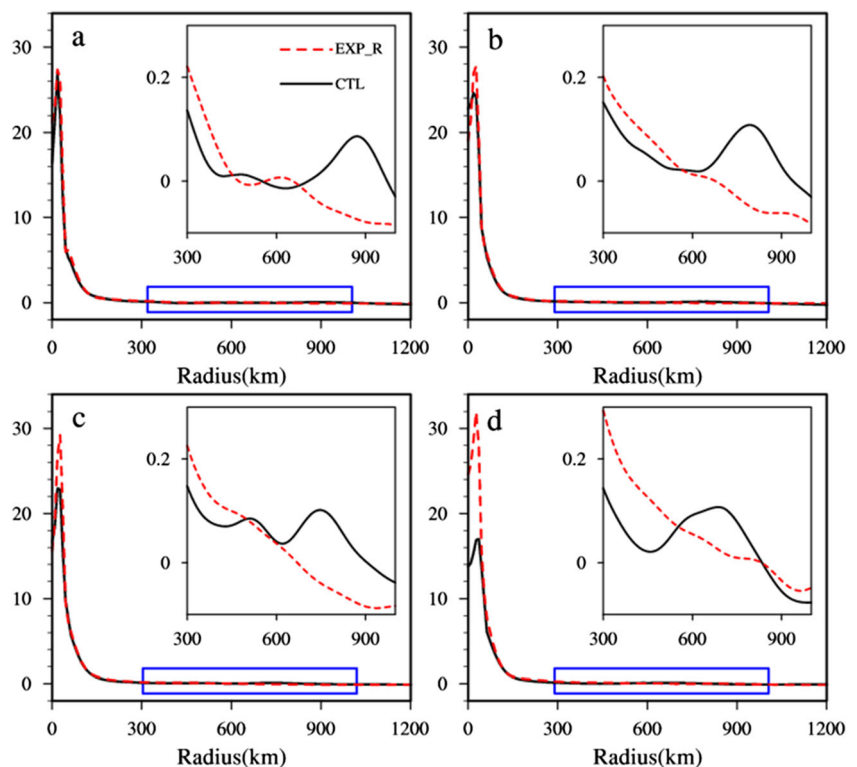


Fig. 14 Evolution of wave-number-1 (a, b, c, d) and 2 (e, f, g, h) vorticity fields (shaded; unit: $1 \times 10^{-5} \text{ s}^{-1}$) in CTL and EXP for (left to right) at 0018 UTC 24 July and 0000 UTC 25 July at the height of $z = 1.5 \text{ km}$

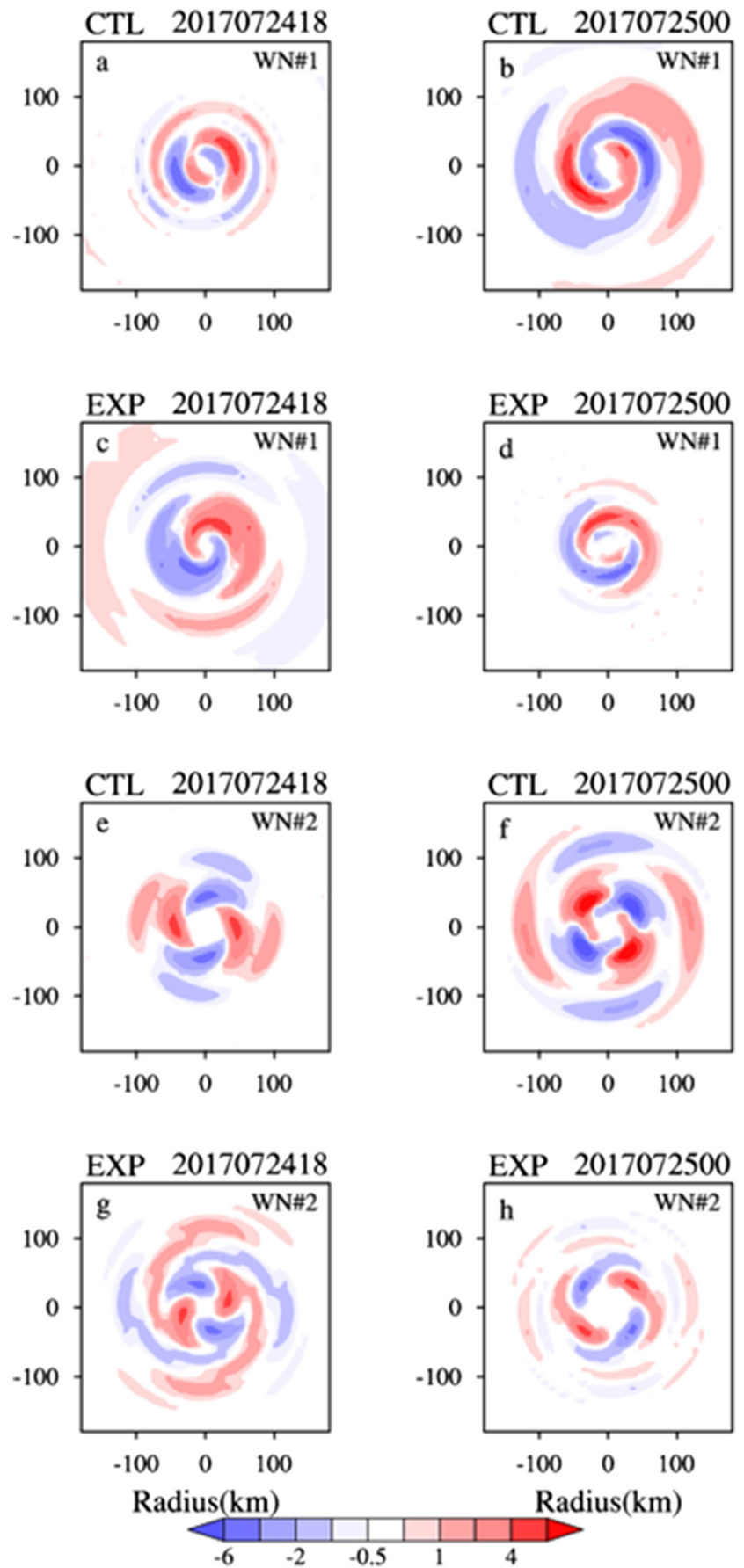
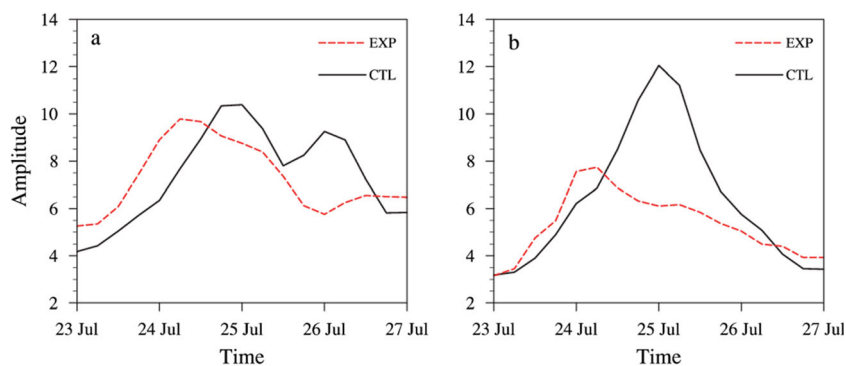


Fig. 15 The amplitude of wave-number-1 (a) and 2 (b) asymmetric vorticity fields (unit: $1 \times 10^{-5} \text{ s}^{-1}$) in CTL (black), EXP (red) during the period of 23 ~ 27 July



- 1) In the presence of Kulap, the competition on the moisture supplies leads to a mid-level dry air layer wrapped around the TC Noru. Meanwhile, a relative stronger VWS is identified. A larger VWS reflects a larger vertical tilting structure, inhibiting TC development. Furthermore, a dry ambient environment favors a low entropy flux entrains downward into boundary layer. As such, the negative impacts of dry air intrusion are pronounced so that TC Noru experiences a weakening stage.
- 2) Dynamically, along with Kulap approaches to Noru, it results in a local vorticity maximum at the outer region of Noru. This local vorticity maximum induces a barotropic instability, by which greatly enhances inner-core asymmetry. The asymmetric perturbations grow at the expense of the mean flow.

Admittedly, this is only a real case study on the weakening of TC intensity during the binary TC interaction. In reality, there are different types of TC intensity change during the mutual interaction. In other words, TC may experience either rapid intensification or decay. The exact processes controlling these intensity changes are not clear yet. It is speculated that the different thermodynamical conditions may partly account for these discrepancies. For instance, the critical separation distance is highly sensitive to the ambient moisture condition. The different separation distance implies varied Fujiwhara effects. In the WNP, the multiple TCs event is prevailing within the MT region where is possibly dynamically unstable. How the MT affects Fujiwhara effect remains unclear, and this topic waits for future studies. Furthermore, our results confirm the recently proposed paradigm for TC intensity modification under vertical wind shear. It emphasizes the need for innovative tools to assess the relative impact of wind shear by each of the TCs. To fulfill these purposes, more experiments are required to disclose the relative roles of the individual storm during the binary TC interaction. These will help gain more insights of the TC intensity change during the multiple TCs event.

Acknowledgements This work was jointly sponsored by the Science and Technology Innovation Project of Ningbo (Grant# 2019B10025), the

National Key R& D Program of China (2017YFC1502000), the National Science Foundation of China (Grant No. 41575056, 41730961, 41775058), and the Priority Academic Program Development of Jiangsu Higher Education Institutions (PAPD).

References

- Brand, S.: Interaction of binary tropical cyclones of the Western North Pacific Ocean. *J. Appl. Meteorol.* **9**(3), 433–441 (1970)
- Braun, S.A.: Reevaluating the role of the Saharan air layer in Atlantic tropical Cyclogenesis and evolution. *Mon. Weather Rev.* **138**(6), 2007–2037 (2010)
- Braun, S.A., Sippel, J.A., Nolan, D.S.: The impact of dry midlevel air on hurricane intensity in idealized simulations with no mean flow. *J. Atmos. Sci.* **69**(1), 236–257 (2012)
- Carr, L.E., Elsberry, R.L.: Objective diagnosis of binary tropical cyclone interactions for the Western North Pacific Basin. *Mon. Weather Rev.* **126**(6), 1734–1740 (1998)
- Carr, L.E., Boothe, M.A., Elsberry, R.L.: Observational evidence for alternate modes of track-altering binary tropical cyclone scenarios. *Mon. Weather Rev.* **125**(9), 2094–2111 (1997)
- Chang, S.W.: A numerical study of the interactions between two tropical cyclones. *Mon. Weather Rev.* **111**(9), 1806–1817 (1983)
- DeMaria, M., Chan, J.C.L.: Comments on “a numerical study of the interactions between two tropical cyclones”. *Mon. Weather Rev.* **112**(8), 1643–1645 (1984)
- Dong, K., Neumann, C.J.: On the relative motion of binary tropical cyclones. *Mon. Weather Rev.* **111**(5), 945–953 (1983)
- Dudhia, J.: Numerical study of convection observed during the winter monsoon experiment using a Mesoscale two-dimensional model. *J. Atmos. Sci.* **46**(20), 3077–3107 (1989)
- Dunion, J.P., Velden, C.S.: The impact of the Saharan air layer on Atlantic tropical cyclone activity. *Bull. Amer. Meteor. Soc.* **85**(3), 353–366 (2004)
- Emanuel, K.A.: The finite-amplitude nature of tropical Cyclogenesis. *J. Atmos. Sci.* **46**(22), 3431–3456 (1989)
- Ferrier, B.: A double-moment multiple-phase four-class bulk ice scheme. Part I: description. *J. Atmos. Sci.* **51**(2), 249–280 (1994)
- Finocchio, P.M., Majumdar, S.J., Nolan, D.S., Iskandarani, M.: Idealized tropical cyclone responses to the height and depth of environmental vertical wind shear. *Mon. Weather Rev.* **144**(6), 2155–2175 (2016)
- Fujiwhara, S.: The natural tendency towards symmetry of motion and its application as a principle in meteorology. *Quart. J. Roy. Meteor. Soc.* **47**(200), 287–292 (1921)
- Fujiwhara, S.: On the growth and decay of vortical systems. *Quart. J. Roy. Meteor. Soc.* **49**(206), 75–104 (1923)
- Fujiwhara, S.: Short note on the behavior of two vortices. *Proc. Phys. Math. Soc. Japan, Ser.* **13**(3), 106–110 (1931)

- Ge, X., Li, T., Peng, M.: Effects of vertical shears and midlevel dry air on tropical cyclone developments. *J. Atmos. Sci.* **70**(12), 3859–3875 (2013)
- Ge, X., Yan, Z., Peng, M., Bi, M., Li, T.: Sensitivity of tropical cyclone track to the vertical structure of a nearby monsoon gyre. *J. Atmos. Sci.* **75**(6), 2017–2028 (2018)
- Gray, W. M.: Tropical cyclone genesis. Colorado State University, Department of Atmospheric Science Paper 234, 121 pp. (1975)
- Gu, J.-F., Tan, Z.-M., Qiu, X.: The evolution of vortex tilt and vertical motion of tropical cyclones in directional shear flows. *J. Atmos. Sci.* **75**(10), 3565–3578 (2018)
- Guimond, S.R., Heymsfield, G.M., Turk, F.J.: Multiscale observations of hurricane Dennis (2005): the effects of hot towers on rapid intensification. *J. Atmos. Sci.* **67**(3), 633–654 (2010)
- Hendricks, E.A., Montgomery, M.T., Davis, C.A.: The role of “Vortical” hot towers in the formation of tropical cyclone Diana (1984). *J. Atmos. Sci.* **61**(11), 1209–1232 (2004)
- Hendricks, E., Peng, M., Ge, X., Li, T.: Performance of a dynamic initialization scheme in the coupled ocean-atmosphere Mesoscale prediction system for tropical cyclones (COAMPS-TC). *Wea. Forecasting*, **26**, 650–663 (2011)
- Holland, G.J., Dietachmayer, G.S.: On the interaction of tropical-cyclone-scale vortices. III: continuous barotropic vortices. *Quart. J. Roy. Meteor. Soc.* **119**(514), 1381–1398 (1993)
- Jang, W., Chun, H.-Y.: Characteristics of binary tropical cyclones observed in the Western North Pacific for 62 years (1951–2012). *Mon. Weather Rev.* **143**(5), 1749–1761 (2015)
- Kain, J.S. and Fritsch, J.M.: Convective parameterization for mesoscale models: the Kain–Fritsch scheme. The representation of cumulus convection in numerical models. *Meteorol. Monogr. No. 46*. Amer. Meteor. Soc., **24** 165–170 (1993)
- Kimball, S.K.: A modeling study of hurricane landfall in a dry environment. *Mon. Weather Rev.* **134**(7), 1901–1918 (2006)
- Kuo, H.-C., Chen, G.T.J., Lin, C.-H.: Merger of tropical cyclones Zeb and Alex. *Mon. Weather Rev.* **128**(8), 2967–2975 (2000)
- Lander, M., Holland, G.J.: On the interaction of tropical-cyclone-scale vortices. I: observations. *Quart. J. Roy. Meteor. Soc.* **119**(514), 1347–1361 (1993)
- Li, T.: In: Oouchi, K., Fudeyasu, H. (eds.) *Synoptic and climatic aspects of tropical cyclogenesis in Western North Pacific*, pp. 61–94. Nova Science Publishers, Hauppauge (2012)
- McBride, J.L., Zehr, R.: Observational analysis of tropical cyclone formation. Part II: comparison of non-developing versus developing systems. *J. Atmos. Sci.* **38**(6), 1132–1151 (1981)
- Miyamoto, Y., Nolan, D.S.: Structural changes preceding rapid intensification in tropical cyclones as shown in a large Ensemble of Idealized Simulations. *J. Atmos. Sci.* **75**(2), 555–569 (2018)
- Miyamoto, Y., Takemi, T.: A transition mechanism for the spontaneous axisymmetric intensification of tropical cyclones. *J. Atmos. Sci.* **70**(1), 112–129 (2013)
- Mlawer, E.J., Taubman, S.J., Brown, P.D., Iacono, M.J., Clough, S.A.: Radiative transfer for inhomogeneous atmospheres: RRTM, a validated correlated-k model for the longwave. *J. Geophys. Res. Atmos.* **102**(D14), 16663–16682 (1997)
- Nolan, D.S.: What is the trigger for tropical cyclogenesis? *Aust. Meteor. Mag.* **56**, 241–266 (2007)
- Onderlinde, M., Nolan, D.: Environmental Helicity and its effects on development and intensification of tropical cyclones. *J. Atmos. Sci.* **71**, 4308–4320 (2014)
- Peng, M.S., Reynolds, C.A.: Sensitivity of tropical cyclone forecasts as revealed by singular vectors. *J. Atmos. Sci.* **63**(10), 2508–2528 (2006)
- Peng, J., Li, T., Peng, M.S., Ge, X.: Barotropic instability in the tropical cyclone outer region. *Quart. J. Roy. Meteor. Soc.* **135**(641), 851–864 (2009)
- Pokhil, A.E., Sitnikov, I.G., Zlenko, V.A., Polyakova, I.V.: Numerical experiments on investigation of atmospheric vortices. *Meteorol. Gidrol.* **4**, 21–28 (1990)
- Prieto, R., McNoldy, B.D., Fulton, S.R., Schubert, W.H.: A classification of binary tropical cyclone-like vortex interactions. *Mon. Weather Rev.* **131**(11), 2656–2666 (2003)
- Riemer, M., Montgomery, M.T., Nicholls, M.E.: Further examination of the thermodynamic modification of the inflow layer of tropical cyclones by vertical wind shear. *Atmos. Chem. Phys.* **13**(1), 327–346 (2013)
- Ritchie, E.A., Holland, G.J.: On the interaction of tropical-cyclone-scale vortices. II: discrete vortex patches. *Quart. J. Roy. Meteor. Soc.* **119**(514), 1363–1379 (1993)
- Schechter, D.A.: Development and nondevelopment of binary Mesoscale vortices into tropical cyclones in idealized numerical experiments. *J. Atmos. Sci.* **73**(3), 1223–1254 (2016)
- Shin, S.-E., Han, J.-Y., Baik, J.-J.: On the critical separation distance of binary vortices in a nondivergent Barotropic atmosphere. *J. Meteor. Soc. Japan, Ser. II.* **84**(5), 853–869 (2006)
- Skamarock, W.C., Klemp, J.B., Dudhia, J., Gill, D.O., Barker, D.M., Duda, M., Huang, X.-Y., Wang, W., Powers, J.G.: A description of the advanced research WRF version 3. NCAR Tech. Note NCAR/TN-4751STR 113 pp. (2008)
- Steranka, J., Rodgers, E.B., Gentry, R.C.: The relationship between satellite measured convective bursts and tropical cyclone intensification. *Mon. Weather Rev.* **114**(8), 1539–1546 (1986)
- Tang, B., Emanuel, K.: A ventilation index for tropical cyclones. *Bull. Amer. Meteor. Soc.* **93**(12), 1901–1912 (2012)
- Wang, Z.: Thermodynamic aspects of tropical cyclone formation. *J. Atmos. Sci.* **69**(8), 2433–2451 (2012)
- Wang, Y., Holland, G.J.: On the interaction of tropical-cyclone-scale vortices. IV: Baroclinic vortices. *Quart. J. Roy. Meteor. Soc.* **121**(521), 95–126 (1995)
- Wang, Y., Rao, Y., Tan, Z.-M., Schönemann, D.: A statistical analysis of the effects of vertical wind shear on tropical cyclone intensity change over the Western North Pacific. *Mon. Weather Rev.* **143**(9), 3434–3453 (2015)
- Wu, L.: Impact of Saharan air layer on hurricane peak intensity. *Geophys. Res. Lett.* **34**(9), L09802 (2007)
- Wu, C.-C., Huang, T.-S., Huang, W.-P., Chou, K.-H.: A new look at the binary interaction: potential Vorticity diagnosis of the unusual southward movement of tropical storm Bopha (2000) and its interaction with Supertyphoon Saomai (2000). *Mon. Weather Rev.* **131**(7), 1289–1300 (2003)
- Wu, L., Braun, S.A., Qu, J.J., Hao, X.: Simulating the formation of hurricane Isabel (2003) with AIRS data. *Geophys. Res. Lett.* **33**(4), L04804 (2006)
- Wu, X., Fei, J., Huang, X., Zhang, X., Cheng, X., Ren, J.: A numerical study of the interaction between two simultaneous storms: Goni and Morakot in September 2009. *Adv. Atmos. Sci.* **29**(3), 561–574 (2012)
- Yan, Z., Ge, X., Peng, M., Li, T.: Does monsoon gyre always favour tropical cyclone rapid intensification? *Quart. J. Roy. Meteor. Soc.* **145**(8), 1–13 (2019)
- Yang, C.-C., Wu, C.-C., Chou, K.-H., Lee, C.-Y.: Binary interaction between typhoons Fengshen (2002) and Fungwong (2002) based on the potential Vorticity diagnosis. *Mon. Weather Rev.* **136**(12), 4593–4611 (2008)
- Yuter, S.E., Houze, R.A.: Three-dimensional kinematic and microphysical evolution of Florida cumulonimbus. Part I: spatial distribution of updrafts, downdrafts, and precipitation. *Mon. Weather Rev.* **123**(7), 1921–1940 (1995)